Promiscuous gating modifiers target the voltage sensor of $K_v7.2$, TRPV1, and H_v1 cation channels

Polina Kornilov,* Asher Peretz,* Yoonji Lee,[†,‡] Karam Son,[†,‡] Jin Hee Lee,[†,‡] Bosmat Refaeli,* Netta Roz,* Moshe Rehavi,* Sun Choi,[†,‡,1] and Bernard Attali*[,1]

*Department of Physiology and Pharmacology, The Sackler Faculty of Medicine, Tel Aviv University, Tel Aviv, Israel; and [†]National Leading Research Laboratory of Molecular Modeling and Drug Design, College of Pharmacy, Graduate School of Pharmaceutical Sciences, and [‡]Global Top5 Research Program, Ewha Womans University, Seoul, Korea

ABSTRACT **Some of the fascinating features of voltage-sensing domains (VSDs) in voltage-gated cation channels (VGCCs) are their modular nature and adaptability. Here we examined the VSD sensitivity of different VGCCs to 2 structurally related nontoxin gating modifiers, NH17 and NH29, which stabilize $K_v7.2$ potassium channels in the closed and open states, respectively. The effects of NH17 and NH29 were examined in Chinese hamster ovary cells transfected with transient receptor potential vanilloid 1 (TRPV1) or $K_v7.2$ channels, as well as in dorsal root ganglia neurons, using the whole-cell patch-clamp technique. NH17 and NH29 exert opposite effects on TRPV1 channels, operating, respectively, as an activator and a blocker of TRPV1 currents (EC_{50} and IC_{50} values ranging from 4 to 40 μM). Combined mutagenesis, electrophysiology, structural homology modeling, molecular docking, and molecular dynamics simulation indicate that both compounds target the VSDs of TRPV1 channels, which, like vanilloids, are involved in π-π stacking, H-bonding, and hydrophobic interactions. Reflecting their promiscuity, the drugs also affect the lone VSD proton channel mVSOP. Thus, the same gating modifier can promiscuously interact with different VGCCs, and subtle differences at the VSD-ligand interface will dictate whether the gating modifier stabilizes channels in either the closed or the open state.—Kornilov, P., Peretz, A., Lee, Y., Son, K., Lee, J. H., Refaeli, B., Roz, N., Rehavi, M., Choi, S., Attali, B. Promiscuous gating modifiers target the voltage sensor of $K_v7.2$, TRPV1, and H_v1 cation channels. *FASEB J.* 28, 2591–2602 (2014). www.fasebj.org**

Key Words: vanilloid · capsaicin · KCNQ

VOLTAGE-GATED CATION CHANNELS (VGCCs) are essential for many vital functions (1–4). Their physiological importance is underscored by the existence of genetic defects, which lead in humans to severe neurological, cardiac, muscular, or metabolic diseases, called channelopathies (1, 2).

VGCCs comprise 4 structural units either connected as a single polypeptide or arranged as 4 separate subunits, which assemble in a tetrameric symmetry around a central ion-conducting pore (5–7). Each subunit possesses 2 main transmembrane modules, a voltage-sensing domain (VSD) and a pore region. VSDs are membrane protein modules endowed with charged amino acids, also called gating charges (6, 8). They undergo conformational changes after alterations of the membrane electric field, thereby inducing motions of the gating charges that could be measured as gating currents (6, 8, 9). Notably, VSDs have also been characterized in voltage-sensitive proteins that lack conventional associated channel pores, such as the voltage-sensitive phosphatase Ci-VSP and voltage-activated proton channels H_v1 and mVSOP (10–12). X-ray crystallographic studies of voltage-gated K^+ (K_v) channels have described the VSD architecture in its activated conformation (13, 14). It is a module of 4 membrane-spanning segments (S1–S4) with the S3b segment and the charge-bearing S4 helix forming a helix-turn-helix structure, termed the paddle motif, which moves at the protein-lipid interface (15, 16). The VSD paddle motifs are modular and transferable structures (16, 17).

So far, the pharmacological toolbox has merely focused on the pore and gate regions of VGCCs. Conversely, the VSD was rarely targeted with small ligand

Abbreviations: CHO, Chinese hamster ovary; cTRPV1, chicken transient receptor potential vanilloid 1; DMEM, Dulbecco's modified Eagle's medium; DMSO, dimethyl sulfoxide; DRG, dorsal root ganglion; GA, genetic algorithm; 5′-IRTX, 5′-iodoresiniferatoxin; K_v, voltage-gated K^+; MD, molecular dynamics; rTRPV1, rat transient receptor potential vanilloid 1; RTX, resiniferatoxin; TRPV1, transient receptor potential vanilloid 1; VGCC, voltage-gated cation channel; VSD, voltage-sensing domain; WT, wild type

[1] Correspondence: B.A., Department of Physiology and Pharmacology, Sackler Medical School, Aviv University, Aviv 69978, Israel. E-mail: battali@post.tau.ac.il; S.C., National Leading Research Laboratory of Molecular Modeling and Drug Design, College of Pharmacy, Graduate School of Pharmaceutical Sciences, and Global Top5 Research Program, Ewha Womans University 120-750, Seoul, Korea. E-mail: sunchoi@ewha.ac.kr

doi: 10.1096/fj.14-250647

This article includes supplemental data. Please visit *http://www.fasebj.org* to obtain this information.

molecules for therapeutic or biophysical purposes, although it is the target of various toxins (18, 19). We recently designed 2 novel diphenylamine carboxylate derivatives, NH17 and NH29, a blocker and an opener of $K_v7.2/K_v7.3$ potassium channels, respectively (20, 21). We found that NH29 is a gating modifier that stabilizes the $K_v7.2$ channel open state by interacting with its VSD. Here we investigated the sensitivity of the VSD to these 2 molecules in different VGCCs.

MATERIALS AND METHODS

Drugs

Details concerning the synthesis and purity of NH29 and NH17 were described previously in Peretz *et al.* (20) as compound 6 and compound 13, respectively. Capsaicin and 5′-iodoresiniferatoxin (5′-IRTX) were purchased from Sigma-Aldrich (Rehovot, Israel) and Alomone Labs (Jerusalem, Israel), respectively. Capsaicin, 5′-IRTX, NH17, and NH29 were dissolved in dimethyl sulfoxide (DMSO) for stock solutions (50 mM), stored at −20°C, and diluted with the recording solution at appropriate concentrations before the experiments to yield the final DMSO concentration of 0.0001–0.1%.

Molecular biology

For expression in mammalian cells, rat transient receptor potential vanilloid 1 (rTRPV1) in pcDNA3 vector was used as the wild-type (WT) template. Site-directed mutagenesis was generated by PCR amplification of WT rTRPV1 using standard PCR techniques with Pfu DNA polymerase (Promega, Madison, WI, USA). All mutant cDNA clones were verified by DNA sequencing.

Chinese hamster ovary (CHO) cell culture and transfection

CHO cells were maintained in Dulbecco's modified Eagle's medium (DMEM) supplemented with 2 mM GlutaMAX (Life Technologies, Inc., Carlsbad, CA, USA), 10% fetal bovine serum, and antibiotics, incubated at 37°C in 5% CO_2. Cells were seeded on poly-L-lysine-coated glass coverslips in a 24-multiwell plate and transiently transfected with TransIT-LT1 Transfection Reagent (Mirus Bio, Madison, WI, USA). pIRES-CD8 was cotransfected as a transfection identification surface marker.

Primary rat dorsal root ganglion (DRG) cultures

DRG neurons were dissected from 0- to 3-d postnatal Sprague-Dawley rats euthanized by decapitation. DRGs were placed in DMEM and dissociated by enzymatic treatment. In brief, after a 30-min incubation in 0.5 mg/ml trypsin type VI, 1 mg/ml collagenase type 1A, and 0.1 mg/ml DNase (Invitrogen/Life Technologies) in Ca^{2+} and Mg^{2+}-free DMEM, the ganglia were centrifuged and resuspended in DMEM with 1.25 mg/ml trypsin inhibitor. After a 5-min incubation, the ganglia were again centrifuged, resuspended in DMEM supplemented with 2 mM GlutaMAX, 10% fetal bovine serum, and penicillin/streptomycin antibiotics and mechanically triturated with a fire-polished glass Pasteur pipette. For electrophysiological recording, dissociated neurons were plated on 13-mm glass coverslips, previously coated with poly-L-lysine (0.5 mg/ml) and collagen (0.25 mg/ml), and used at 1–4 d in culture.

Electrophysiology

For transfected CHO cells, recordings were performed 40 h after transfection, using the voltage-clamp configuration of the whole-cell patch-clamp technique. Transfected cells were visualized using anti-CD8 antibody-coated beads. Data were sampled at 5 kHz and low pass filtered at 2 kHz (Axopatch200B amplifier with pClamp10 software and a 4-pole Bessel low pass filter; Molecular Devices, Sunnyvale, CA, USA). For $K_v7.2$ current recordings, the patch pipettes were pulled from borosilicate glass (Warner Instruments, Hamden, CT, USA) with a resistance of 3−7 MΩ and were filled with 130 mM KCl, 5 mM Mg ATP, 5 mM EGTA, and 10 mM HEPES, pH 7.3 (adjusted with KOH), and sucrose was added to adjust osmolarity to 290 mOsmol. The external solution contained 140 mM NaCl, 4 mM KCl, 1.2 mM $MgCl_2$, 1.8 mM $CaCl_2$, 11 mM glucose, and 5.5 mM HEPES, pH 7.3 (adjusted with NaOH), and sucrose was added to adjust osmolarity to 310 mOsmol. For transient receptor potential vanilloid 1 (TRPV1) current recordings, the solutions were the same as those used for $K_v7.2$, except that the extracellular solution contained no $CaCl_2$ to limit desensitization and included 1 mM EGTA and 1 mM $MgCl_2$. For proton-evoked TRPV1 currents, the external solution contained 140 mM NaCl, 4 mM KCl, 1 mM $MgCl_2$, 11 mM glucose, and 5.5 mM 2-(*N*-morpholino)ethanesulfonic acid (MES), pH 5−6.4 (adjusted with HCl). For recordings of mVSOP proton currents, the external solution contained 100 mM NaCl, 4 mM KCl, 1.2 mM $MgCl_2$, 1.8 mM $CaCl_2$, and 100 mM HEPES, pH 7 (adjusted with NaOH). The patch pipettes were filled with 100 mM KCl, 3 mM $MgCl_2$, and 100 mM HEPES, pH 7 (adjusted with KOH). For voltage-clamp recordings in DRG neurons, the extracellular and intracellular solutions were the same as those used to record $K_v7.2$ currents in CHO cells. For current-clamp recordings in DRG neurons, the patch pipettes were filled with 135 mM KCl, 1 mM K_2ATP, 1 mM MgATP, 2 mM EGTA, 1.1 mM $CaCl_2$, 5 mM glucose (free $[Ca^{2+}]_i$=87 nM), and 10 mM HEPES, adjusted with KOH at pH 7.4 (315 mOsmol). The external solution contained 150 mM NaCl, 2.5 mM KCl, 2 mM $CaCl_2$, 2 mM $MgCl_2$, 15 mM glucose, and 10 HEPES, adjusted with NaOH at pH 7.4 (325 mOsmol). Drug exposure was evoked by rapid application using a fast perfusion system (AutoMate Scientific, Berkeley, CA, USA).

Data analysis

Data analysis was performed using the Clampfit program (pClamp10), Microsoft Excel (Microsoft, Richmond, WA, USA), and Prism 5.0 (GraphPad Software, Inc., San Diego, CA, USA). Conductance (G) was calculated as $G = I/(V - V_{rev})$. G was then normalized to the maximal conductance. Activation curves were fitted to a single Boltzmann distribution according to $G/G_{max} = 1/\{1 + \exp[(V_{50} - V)/s]\}$, where V_{50} is the voltage at which the current is half-activated and s is the slope factor. Dose-response curves were fitted to a sigmoidal dose-response (variable slope) according to $1/(1+10^{((\log EC_{50}-X))} \cdot n_H)$. All data are expressed as means ± SEM. Statistically significant differences were assessed by unpaired t tests for 2 samples assuming unequal variances for comparing WT with mutant channels and by paired t tests of the means for comparing the effect of a drug before and after its application in the same cell.

Molecular docking

The 3-dimensional structures of the ligands were generated by Concord and energy minimized using MMFF94s force field and MMFF94 charges until the root mean square of the Powell gradient was 0.05 kcal · mol^{-1} · A^{-1} in SYBYL-X 1.2 (Tripos International, St. Louis, MO, USA). The homotetrameric homology model of rTRPV1, which we constructed previously (20) was used as a protein structure. The flexible docking study on the rTRPV1 model was performed using GOLD 5.0.1 (Cambridge Crystallographic Data Centre, Cambridge, UK), which uses a genetic algorithm (GA) and allows for full ligand flexibility and partial protein flexibility. The binding site was defined as 10 Å around the capsaicin, complexed in the rTRPV1 model. The side chains of the 7 residues (*i.e.*, Tyr511, Ser512, Leu515, Phe543, Thr550, Asn551, and Thr556), which are thought to be important for ligand binding, were set to be flexible with "crystal mode" in GOLD. The ligands were docked using the GoldScore scoring function with 50 GA runs, and other parameters were set as default. The computational calculations were undertaken on an Intel Xeon Quad-core workstation with Linux CentOS 5.5.

Model refinement using molecular dynamics (MD) simulation

The docked complexes were refined by molecular dynamics (MD) simulation using the NAMD 2.8 package. The explicit membrane system was constructed by placing the palmitoyloleoylphosphatidylcholine molecules surrounding the transmembrane region, which was predicted by the Add Membrane and Orient Molecule protocol in Discovery Studio 2.5 (Accelrys Inc., San Diego, CA, USA). Then, the receptor in the membrane system was solvated with the explicit water molecules and ionized with 150 mM KCl. The whole system was energy minimized in the order of lipid membrane, waters, and the entire molecules, followed by heating, equilibration, and production runs for 20 ns. The MD production runs were performed in the supercomputer of the Korea Institute of Science and Technology Information (Yusong, Korea).

RESULTS

Contrasting effects of compound NH29 on K_v7.2 and TRPV1 channels

We previously designed the diphenylamine carboxylate derivative, NH29 (**Fig. 1*A***), and found that it acts as a gating modifier, activating K_v7.2/K_v7.3 channels (20, 21). Here we show that NH29 exerts opposite effects on K_v7.2 and TRPV1 channels. When initially examined in transfected CHO cells expressing K_v7.2 homomeric channels, external application of 25 μM NH29 rapidly increased K_v7.2 K^+ currents at threshold potentials (Fig. 1*B*). At −40 mV, NH29 enhanced K_v7.2 current amplitude by 3.5 ± 0.3-fold with an EC_{50} = 14 ± 2 μM (n=15, P<0.01; ref. 21). The increase in K_v7.2 current mostly resulted from a left shift of the voltage dependence of channel activation (ΔV_{50}=−15.5 mV; Fig. 1*C*). In contrast to its activating effect on K_v7.2 channels, NH29 intriguingly inhibited rTRPV1 currents expressed in CHO cells. NH29 (50 μM) reversibly inhibited rTRPV1 currents evoked by the fast application of 0.5 μM capsaicin (86±2% inhibition; n=7, P<0.001; Fig. 1*D*), with an IC_{50} of 4.2 ± 1.4 μM (n=5–11; Fig. 1*E*). NH29 could also inhibit rTRPV1 currents evoked by protons (90±2% inhibition with 50 μM NH29 at pH 6.4; n=11, P<0.01; see **Fig. 5*A*−*C***). NH29 not only inhibited recombinant rTRPV1 currents expressed in CHO cells but potently and reversibly blocked native TRPV1 currents evoked by capsaicin (1 μM) in rat sensory DRG neurons (at 50 μM, 72±5% inhibition, n=6; P<0.01; Fig. 1*F*). Thus, by activating K_v7.2 and inhibiting TRPV1 channels, NH29 is expected to dampen neuronal excitability. As shown in Fig. 1*G*, 25 μM NH29 hyperpolarized the resting membrane potential (from −56.0±2.0 to −65.0±2.2 mV; n=9; P<0.01) and reversibly reduced the frequency of spike discharge evoked in DRG neurons.

Next, we studied the voltage-dependence of TRPV1 current inhibition by NH29. When TRPV1 currents were solely evoked by voltage steps from −100 to +100 mV, NH29 (50 μM) was ineffective (**Fig. 2*A, B***). In contrast, NH29 was a potent blocker of TRPV1 currents evoked by 10 nM capsaicin (Fig. 2*C, D*), and its inhibitory effect was somewhat voltage dependent, with a stronger inhibition at hyperpolarized potentials (~62–70% inhibition) than at depolarized potentials (~50% inhibition). As shown previously (22–24), capsaicin induced a marked left shift of the voltage dependence of TRPV1 activation (ΔV_{50}=~−120 mV). Notably, NH29 acted as a gating modifier, by producing a powerful right shift (+172 mV) of the capsaicin-induced TRPV1 activation curve (V_{50}=15.8±3.0 mV, V_{50}=−105.3±12.7 mV, and V_{50}=67.5±3.4 mV for TRPV1 currents evoked by voltage alone, in the presence of 10 nM capsaicin, and in the presence of 10 nM capsaicin+50 μM NH29, respectively; n=4; Fig. 2*E*).

Contrasting effects of compound NH17 on K_v7.2 and TRPV1 channels

Compound NH17 shares with NH29 the diphenylamine moiety but differs by its aromatic ring nitro substituents and its positively charged quaternary amine branched group (**Fig. 3*A***). When initially examined in CHO cells expressing K_v7.2 homomeric channels, external application of 25 μM NH17 blocked the K_v7.2 currents by >80% (IC_{50}=10 μM), with no significant difference in the conductance-voltage relationship (Fig. 3*B, C*). Notably, NH17 produced an opposite effect on TRPV1 channels at negative membrane potentials. By holding transfected CHO cells at −60 mV, NH17 (50 μM) evoked by itself TRPV1 inward currents (Fig. 3*D*) with an EC_{50} of 43 ± 16 μM (n=5–7; Fig. 3*F*). NH17 evoked no currents in nontransfected CHO cells. The direct activation of rTRPV1 currents by NH17 was potently blocked by 1 μM 5′-IRTX, a TRPV1-selective antagonist (84±6% inhibition; n=8; P<0.05; Fig. 3*E*), which confirms that the currents evoked by NH17 are specifically flowing through TRPV1 channels. NH17 exerted a sensitizing effect when TRPV1 currents were evoked by 10 nM capsaicin. The capsaicin-induced currents were enhanced by 370 ± 26% in the presence

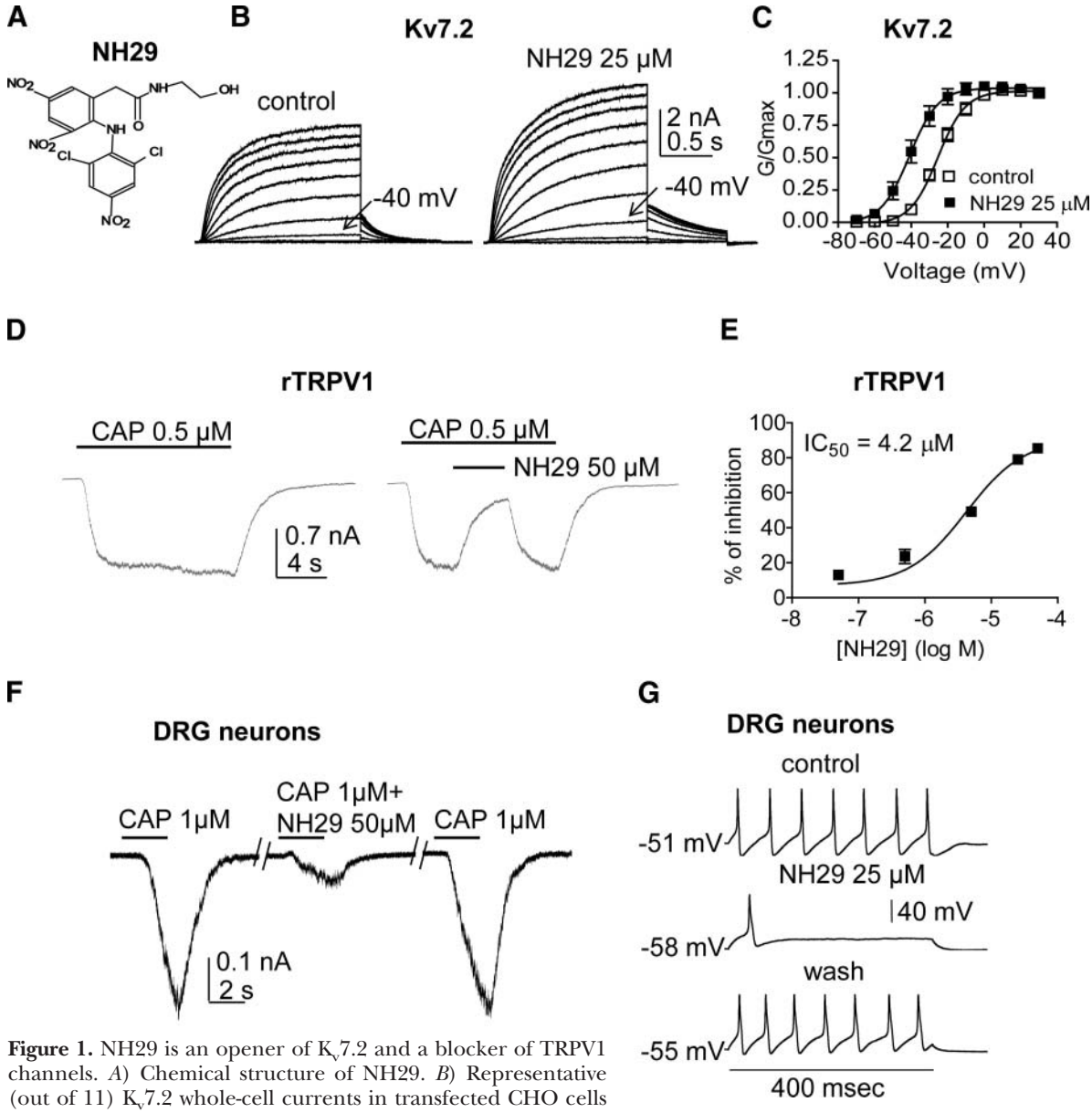

Figure 1. NH29 is an opener of $K_v7.2$ and a blocker of TRPV1 channels. *A*) Chemical structure of NH29. *B*) Representative (out of 11) $K_v7.2$ whole-cell currents in transfected CHO cells in the absence (control) and presence of 25 μM NH29. Cells were held at −90 mV and stepped for 1.5 s from −70 to +30 mV in 10-mV increments and repolarized at −60 mV. *C*) The normalized conductance was plotted as a function of the test voltages, for cells in the absence (control, open squares) and presence (solid squares) of 25 μM NH29 (n=15). *$P < 0.01$. *D*) Representative (out of 7) rTRPV1 whole-cell currents activated by 0.5 μM capsaicin (CAP, left panel) and reversibly inhibited by 50 μM NH29 (right panel) in transfected CHO cells (holding potential −60 mV). *E*) Dose response of NH29 inhibition of capsaicin-induced rTRPV1 currents yielded an IC_{50} of 4.2 ± 0.3 μM (n=5–11). *F*) Representative (out of 7) rat DRG neuron whole-cell currents activated by 1 μM capsaicin and reversibly inhibited by 50 μM NH29 (holding potential −60 mV). *G*) Representative (out of 12) rat DRG spiking discharge evoked by a squared depolarizing current pulse (100 pA for 400 ms) before (control), during exposure to 25 μM NH29 and after washout (wash).

of 50 μM NH17, with an EC_{50} of 40 ± 8 μM (n=8; P<0.05; Fig. 3*D*). The NH17 sensitizing action was not only mirrored by an increased current amplitude but was also reflected by faster activation kinetics with an accelerated half-time to peak ($t_{1/2}$=5.5±0.3 and $t_{1/2}$= 4.5±0.5 a for 10 nM capsaicin in the absence or presence of 50 μM NH17, respectively; n=10; P<0.05). NH17 not only activated by itself recombinant rTRPV1 currents expressed in CHO cells but also evoked native TRPV1 currents in rat DRG neurons held at −60 mV; this activation was also blocked by 1 μM 5′-IRTX (Fig. 3*G*), indicating that the inward current evoked by NH17 flowed through native TRPV1 channels. Thus, by blocking $K_v7.2$ channels and activating TRPV1 currents at nearly resting membrane potentials, NH17 is presumed to increase neuronal excitability. By current clamp we measured the effect of NH17 on DRG neuronal excitability (Fig. 3*H*). A single spike discharge pattern was evoked by injecting a minimal depolarizing current pulse (~10 pA, 400 ms). External application of 1 μM NH17 depolarized the DRG membrane potential (ΔV=+7±1 mV; n=5) and increased the number

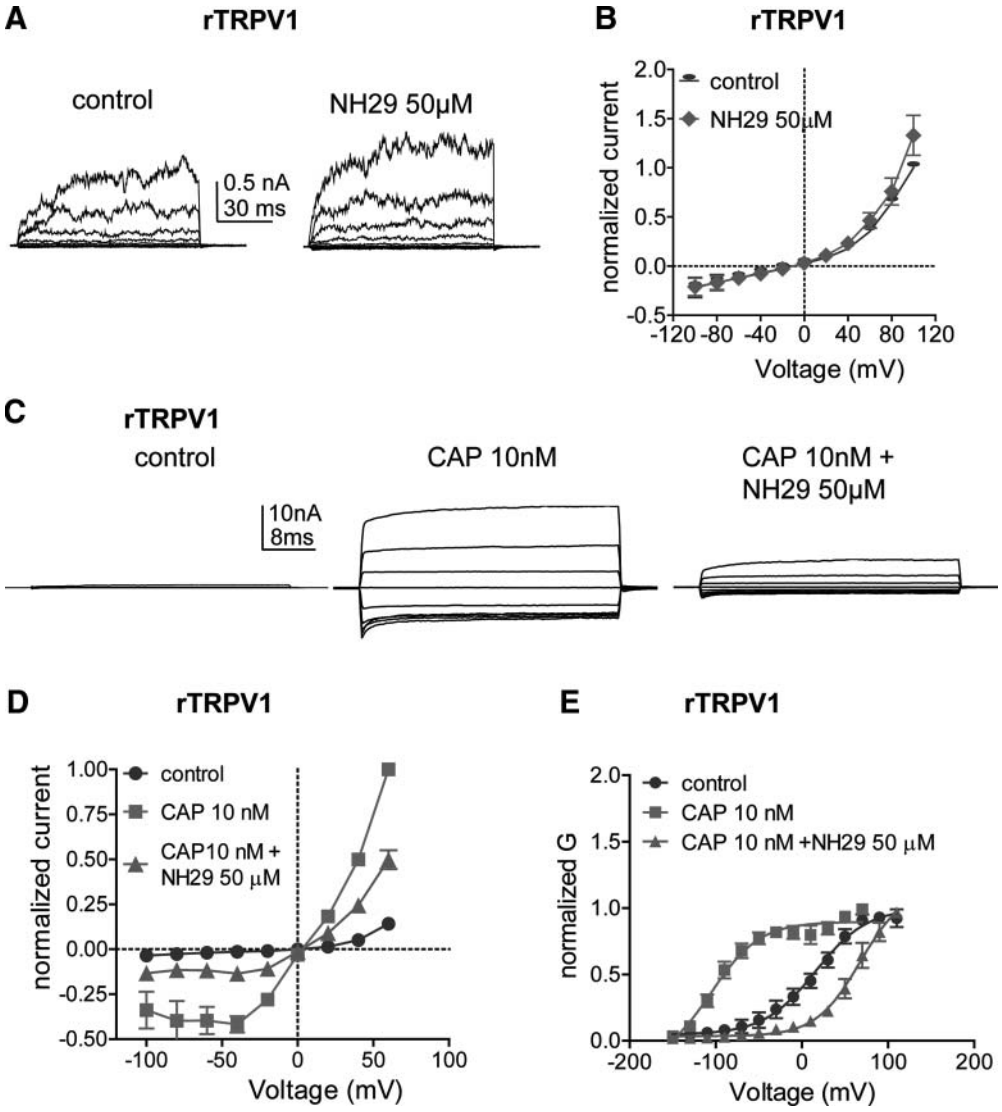

Figure 2. Effect of NH29 on the voltage dependence of rTRPV1 currents expressed in transfected CHO cells. *A*) Representative (out of 5) rTRPV1 whole-cell currents exclusively evoked by voltage, in the absence (control) and presence of 50 μM NH29. Cells, held at −60 mV, were stepped for 100 ms from −100 to +100 mV in 20-mV increments. *B*) Normalized rTRPV1 *I–V* relations in the absence (circles) and presence of 50 μM NH29 (diamonds; n=5). Current was normalized to that obtained in control at +100 mV. *C*) Representative (out of 14) rTRPV1 whole-cell currents recorded in control solution (left panel) in the presence of 10 nM capsaicin (CAP, middle panel) and in the presence of 10 nM capsaicin + 50 μM NH29 (right panel). Cells held at −60 mV were stepped for 40 ms from −100 mV to +60 mV in 20-mV increments. *D*) Normalized rTRPV1 *I–V* relations in control solution (circles) in the presence of 10 nM capsaicin (squares) and in the presence of 10 nM capsaicin + 50 μM NH29 (triangles; n=14; *P<0.01, significantly different from capsaicin alone). Current was normalized to that obtained in 10 nM capsaicin at +60 mV. *E*) Normalized rTRPV1 conductance (*G*)-voltage relations in control solution (circles) in the presence of 10 nM capsaicin (squares) and in the presence of 10 nM capsaicin + 50 μM NH29 (triangles; n=4).

of evoked spikes. The hyperexcitability discharge pattern induced by NH17 was so strong that in some cases, it could lead DRG neurons to fire spontaneously, with no need to inject depolarizing current (Fig. 3*H*).

Next, we examined the voltage dependence of NH17 effects on TRPV1 currents in transfected CHO cells. We first studied the current-voltage (*I–V*) relations of TRPV1 currents evoked by voltage in the absence and presence of NH17. In fact, NH17 exhibited a dual effect on TRPV1 channels with a doubly rectifying *I–V* shape. The activating effect of NH17 was sharply voltage dependent, because NH17 evoked TRPV1 currents only between −100 and +40 mV (**Fig. 4*A*, *B***). At potentials positive to +40 mV, NH17 inhibited TRPV1 currents by up to 70% inhibition at +100 mV. NH17 acted as a gating modifier, thus producing a marked left shift (>−150 mV) of the voltage-dependent TRPV1 activation curve (Fig. 4*E*). Indeed, a Boltzmann fit of the conductance-voltage relation made between −50 to −150 mV, yields a V_{50} of −111 ± 1 mV (n=5). Then, we examined the *I–V* relations of TRPV1 currents evoked by 10 nM capsaicin in the absence and presence of NH17 (Fig. 4*C*, *D*). We found that the sensitizing effect of NH17 was also sharply voltage-dependent and only

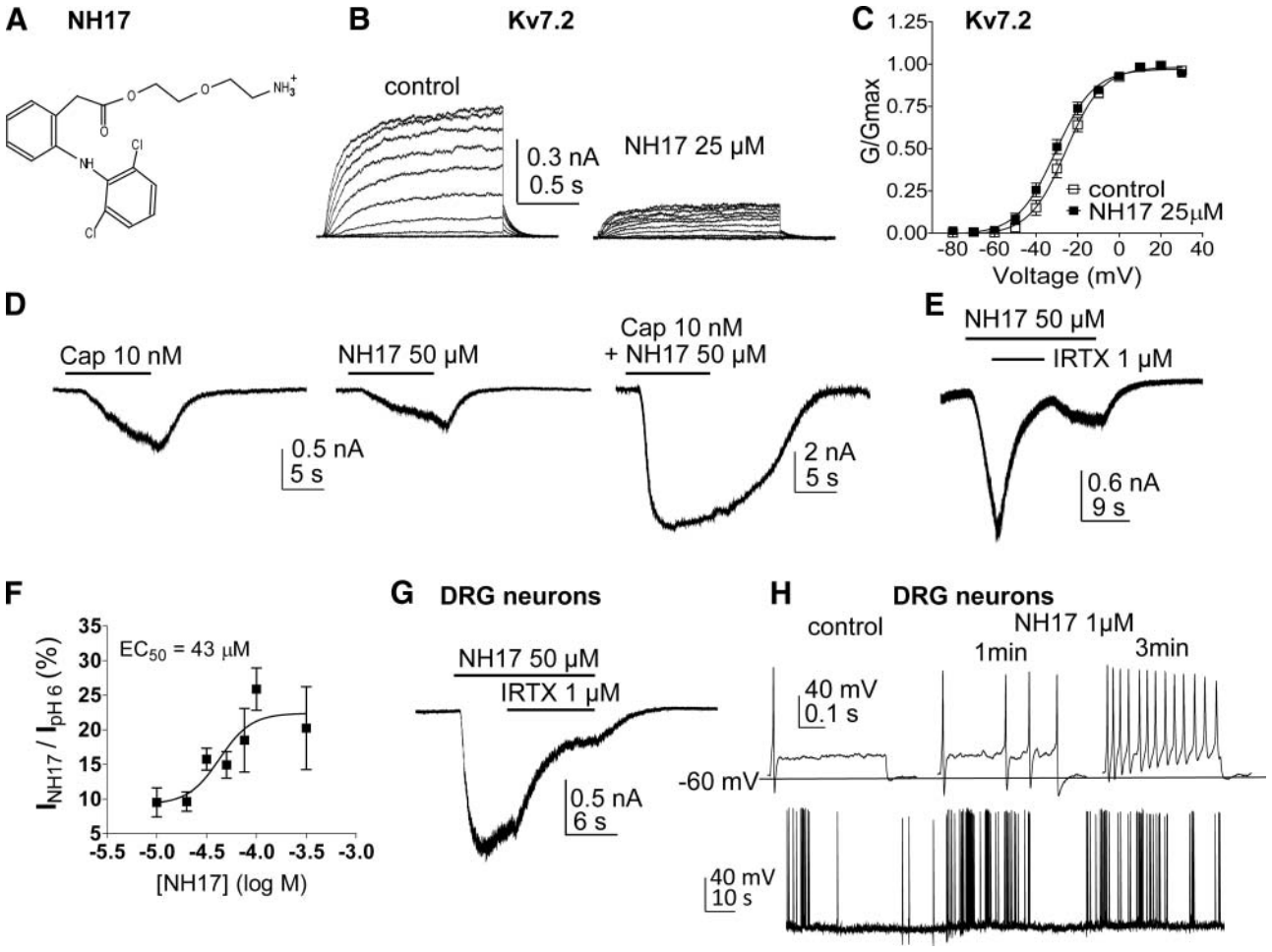

Figure 3. NH17 is a blocker of $K_v7.2$ and an activator of TRPV1 channels. *A*) Chemical structure of NH17. *B*) Representative (out of 11) $K_v7.2$ whole-cell currents recorded in transfected CHO cells in the absence (control) and presence of 25 μM NH17. Cells were held at −90 mV and stepped for 1.5 s from −80 mV to +30 mV in 10-mV increments and repolarized at −60 mV. *C*) Normalized $K_v7.2$ conductance-voltage relations in the absence (open squares) and presence of 25 μM NH17 (solid squares; n=11). *D*) Representative (out of 10) rTRPV1 whole-cell currents recorded in transfected CHO cells at −60 mV. From left to right: currents were evoked by 10 nM capsaicin, 50 μM NH17, and 10 nM capsaicin + 50 μM NH17. *E*) NH17-induced rTRPV1 current was potently blocked by 1 μM IRTX, a TRPV1-selective antagonist (n=8; P<0.01). *F*) Dose response of NH17-induced rTRPV1 currents yielded an EC_{50} of 43 μM (n=5–7). *G*) Representative (out of 4) rat DRG neuron whole-cell currents evoked by 50 μM NH17 and inhibited by 1 μM IRTX (holding potential −60 mV). *H*) Top panel, representative (out of 5) rat DRG spiking discharge, evoked by a squared depolarizing current pulse (10 pA for 400 ms) before (control) and during exposure to 1 μM NH17 for 1 and 3 min; bottom panel, representative trace of spontaneously spiking DRG neuron previously exposed (5 min) to 1 μM NH17 (n=7).

occurred at negative potentials from −100 to −40 mV. At >0 mV, NH17 was a potent blocker of capsaicin-evoked TRPV1 currents, reaching >85% inhibition at +80 mV.

TRPV1 residues involved in NH29-mediated inhibition

We searched for potential residues involved in TRPV1 modulation by NH29. We previously showed that NH29 stabilizes the $K_v7.2$ channel open state by interacting with its VSD (21). As for $K_v7.2$, NH29 also modulates TRPV1 channels as a gating modifier but in an opposite way, hence producing a powerful right shift of the capsaicin-induced TRPV1 conductance-voltage relation. Therefore, we hypothesized that the VSD of TRPV1, like that of $K_v7.2$, could be a possible target of NH29. We performed an alanine mutagenesis of several residues spanning the segments S3 and S4 and the linker S4−S5 of the VSD. In addition, 2 negatively charged amino acids were neutralized (Fig. 5*A*). Because capsaicin is known to interact with the so-called vanilloid pocket formed by the VSD segments S3 and S4 (25–28), the currents of WT rTRPV1 and of all mutants were evoked by protons (at pH 6.4, except for mutant Y511A at pH 6). The proton-interacting region was previously shown to involve a site located in the external vestibule of the channel pore (29). Thus, proton activation of rTRPV1 should prevent any bias of the VSD mutations on capsaicin-induced currents. Among the various TRPV1 mutants tested in transfected CHO cells, mutants S510A, Y511A in S3a, K535A in linker S3−S4, and T550A in S4 were significantly less sensitive

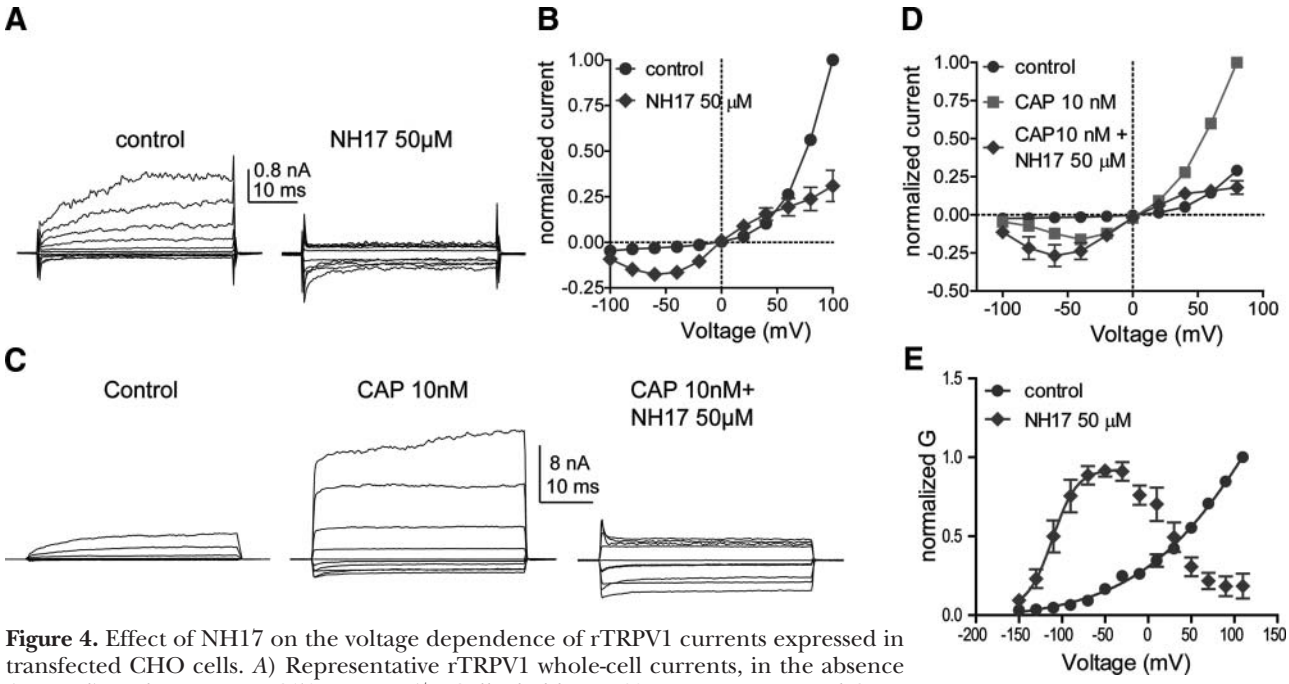

Figure 4. Effect of NH17 on the voltage dependence of rTRPV1 currents expressed in transfected CHO cells. *A*) Representative rTRPV1 whole-cell currents, in the absence (control) and presence of 50 μM NH17. Cells, held at −60 mV, were stepped from −100 to +100 mV in 20-mV increments and repolarized at −60 mV. *B*) Normalized rTRPV1 *I–V* relations in the absence (circles) and presence of 50 μM NH17 (diamonds; n=16). Current was normalized to that obtained in control at +100 mV. *$P < 0.01$ *vs.* control. *C*) Representative (out of 9) rTRPV1 whole-cell currents recorded in control solution (left panel), in the presence of capsaicin 10 nM (middle panel), and in the presence of 10 nM capsaicin + 50 μM NH17 (right panel). Cells, held at −60 mV, were stepped for 40 ms from −100 to +80mV in 20-mV increments. *D*) Normalized rTRPV1 *I–V* relations in control solution (circles), in the presence of 10 nM capsaicin (squares), and in the presence of 10 nM capsaicin + 50 μM NH17 (diamonds; n=9). Current was normalized to that obtained in 10 nM capsaicin at +80 mV. *$P < 0.01$ *vs.* capsaicin alone. *E*) Normalized rTRPV1 conductance (*G*)-voltage relations in control solution (circles) and in the presence of 50 μM NH17 (diamonds; n=5). Conductance was normalized to that obtained in control at +110 mV.

to the inhibitory effect of 50 μM NH29 than WT (68±3, 0±0, 37±4, and 74±2% inhibition, for mutants S510A, Y511A, K535A, and T550A, respectively, compared with 90±2% inhibition for WT; at −60 mV, pH 6.4; n=6–13; P<0.01; Fig. 5*A*, *B*). Notably, the capsaicin-insensitive mutant Y511A (27) was virtually resistant to NH29 inhibition at negative potentials and exhibited a much weaker inhibition at positive potentials (70 and 43% inhibition for WT and Y511A, respectively; at +80 mV, pH 6.4; n=4; P<0.01; Fig. 5*C*). When the VSD mutants were screened for capsaicin-evoked currents, nearly the same mutations (Y511A and K535A) were significantly less sensitive to the inhibitory effect of NH29 than WT (Supplemental Fig. S1*A*), whereas additional mutants were virtually insensitive (Y530A in S3b) or hypersensitive (S520A in S3a and R534A in linker S3−S4) to NH29 inhibition (Supplemental Fig. S1*A*, *B*). Birds express a vanilloid-insensitive homolog of TRPV1 (27). Because the insensitivity of chicken transient receptor potential vanilloid 1 (cTRPV1) to capsaicin relative to that of mammalian orthologs (rat and human) was ascribed to a difference in ~8 amino acids in the VSD at the vicinity of segments S3 and S4 (27), we checked the sensitivity of cTRPV1 to NH29 inhibition when currents were evoked by protons (at pH 6). The cTRPV1 was totally insensitive to NH29 inhibition both at negative and positive potentials (**Fig. 6*A, B***).

TRPV1 residues involved in NH17-mediated modulation

Because NH17 acted on TRPV1 channels as a gating modifier by producing at negative potentials a potent left shift of the voltage-induced TRPV1 activation, we assumed that the VSD of TRPV1 could be, as for NH29, a possible target of NH17. Using the same VSD mutants, we first examined the ability of NH17 (50 μM) to induce by itself a TRPV1 current at −60 mV (**Fig. 7*A***). In 3 mutants (Y511A, Y530A, and M547A), NH17 was unable to elicit any current at −60 mV; however, it could still inhibit the current evoked at positive voltages (Fig. 7*B, C*). In other mutants (T550A and T556A), NH17 evoked significantly smaller currents than those of WT at −60 mV. Notably, in mutant T556A, NH17 was unable, as in WT, to evoke currents at negative voltages and to inhibit currents induced at positive potentials (Fig. 7*D*). In one mutant, S532A in S3b, NH17 evoked significantly larger currents than WT at −60 mV (Fig. 7*A*). We also examined the sensitivity of cTRPV1 to NH17 modulation when currents were evoked by protons (at pH 6). Unlike rTRPV1, cTRPV1 was barely sensitive to NH17 modulation regarding either its activating effect at negative potentials or its inhibition at positive voltages (Fig. 6*C*−*G*). When currents were exclusively evoked by voltage (not by protons), cTRPV1 was totally insensitive to NH17 activation at negative

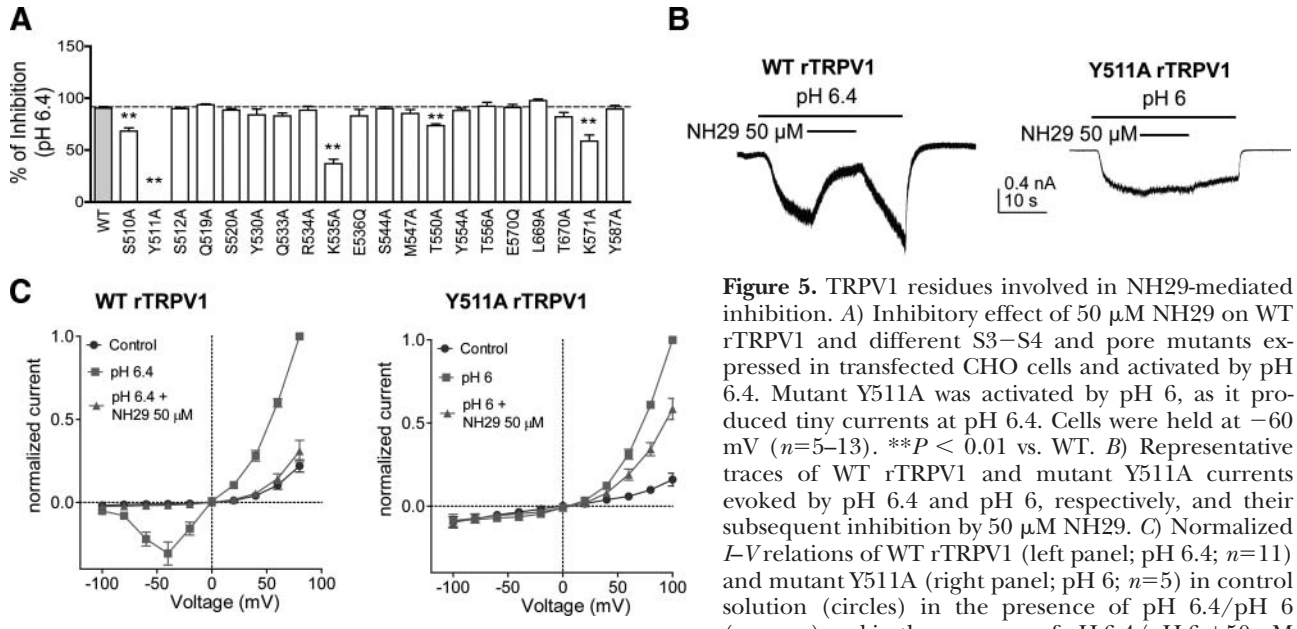

Figure 5. TRPV1 residues involved in NH29-mediated inhibition. *A*) Inhibitory effect of 50 μM NH29 on WT rTRPV1 and different S3−S4 and pore mutants expressed in transfected CHO cells and activated by pH 6.4. Mutant Y511A was activated by pH 6, as it produced tiny currents at pH 6.4. Cells were held at −60 mV (n=5–13). $^{**}P < 0.01$ vs. WT. *B*) Representative traces of WT rTRPV1 and mutant Y511A currents evoked by pH 6.4 and pH 6, respectively, and their subsequent inhibition by 50 μM NH29. *C*) Normalized *I–V* relations of WT rTRPV1 (left panel; pH 6.4; n=11) and mutant Y511A (right panel; pH 6; n=5) in control solution (circles) in the presence of pH 6.4/pH 6 (squares) and in the presence of pH 6.4/pH 6 +50 μM NH29 (triangles). For WT rTRPV1, currents were normalized to pH 6.4 at +80 mV, whereas for Y511A mutant, currents were normalized to pH 6 at +100 mV. $^{*}P < 0.01$ *vs.* pH 6.4 or pH 6 alone.

potentials and much less sensitive to NH17 inhibition at positive voltages (Fig. 6*C, D*).

Docking studies of NH29 and NH17 to a tetrameric homology model of rTRPV1

Taken together, the results suggest that NH29 and NH17 interact with the VSD of the rTRPV1 channel. Considering the experimental constraints of our mutagenesis study, we performed a flexible docking study of NH29 and NH17 to a tetrameric homology model of rTRPV1, which we recently characterized (30). Using this model, we previously showed that the vanilloid drugs, capsaicin and resiniferatoxin (RTX), bind to a site that lies in segments S3 and S4 of the VSD of one subunit and near the pore domain of an adjacent subunit (30). The binding site formed a deep bottom hole surrounded by Tyr511, Tyr565, and Lys571 and an upper hydrophobic region composed of Phe543 and Met547. Whereas the vanillyl moiety was found to engage in π-π stacking and hydrophobic interactions with Tyr511 and H bonding with Ser512, the hydrophobic nonenyl tail of capsaicin and the C13-propenyl group of RTX contributed to hydrophobic interactions with Met547 (30).

The docking results showed that both NH17 and NH29 bind well to our TRPV1 model, occupying the vanilloid binding pocket. The docked complexes with the best docking fitness scores were selected and further refined by MD simulation and energy minimization in the explicit membrane and solvated system. The binding mode of NH17 showed that the dichloroaniline ring occupied the vanilloid binding site in TRPV1, producing π-π stacking and hydrophobic interactions with Tyr511 (**Fig. 8*A, B,*** left). The amino group connecting the 2 phenyl rings also interacts with Tyr511 *via* H bonding. The positively charged quaternary amine group could make electrostatic interactions along with H bonding with Glu570 and Leu669. Hence, to retrospectively validate the docking mode of NH17 to rTRPV1, we probed whether NH17 could, as in WT, evoke by itself a current in mutant L669A located in segment S6 of the pore region. Figure 7*A* shows that NH17 evoked in mutant L669A significantly smaller currents than those in WT at −60 mV (18±4 *vs.* 93±13 pA/pF for L669A and WT, respectively; n=15; P<0.01). Thus, the docking and mutagenesis data suggest that Leu669, located at the adjacent subunit, plays an important role in ligand binding and also confirm that ligand docking occurs between 2 subunits. For NH29, the dichloronitrophenyl ring resided in the vanilloid binding site, producing π-π stacking and hydrophobic interactions with Tyr511 (Fig. 8*A, B*, right). Notably, the terminal −OH functionality is engaged in H bonding with the $-NH3^{+}$ group of Lys571. Thus, we retrospectively validated the docking mode of NH29 to rTRPV1 by probing the effect of NH29 on currents evoked by protons in mutant K571A in linker S4−S5 (Fig. 5*A*). Results showed that mutant K571A was significantly less sensitive to the inhibitory effect of 50 μM NH29 than WT (59±6 and 90±2% inhibition for K571A and WT, respectively; at −60 mV, pH 6.4; n=13; P<0.01; Fig. 5*A*).

DISCUSSION

Modularity, adaptability, and promiscuity represent the most intriguing features of VSDs (16, 17, 31, 32). Structurally diverse gating modifier toxins interact with the relatively conserved VSDs of different VGCCs (18, 19). On the one hand, different structural classes of

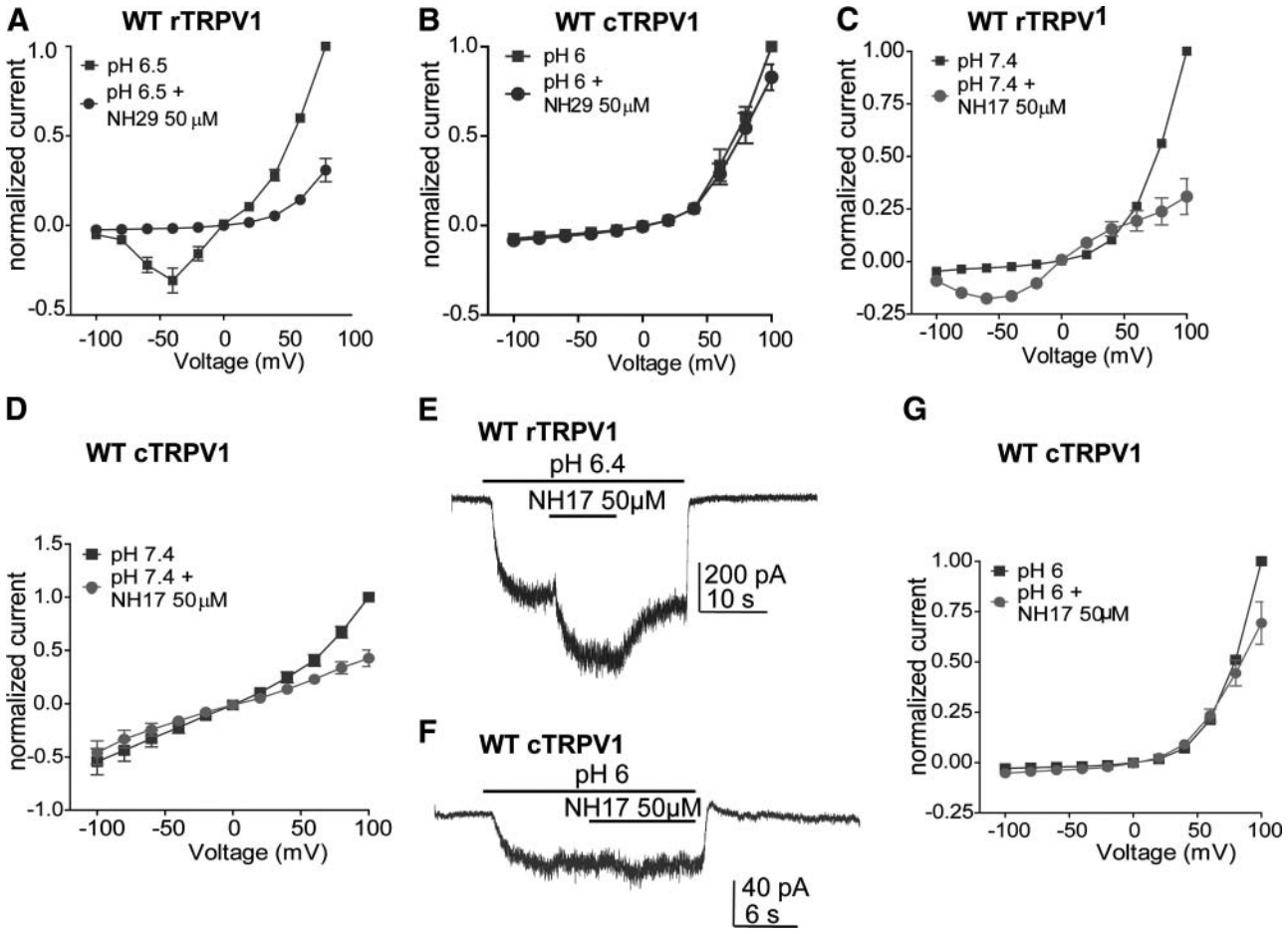

Figure 6. Comparative rTRPV1 and cTRPV1 sensitivity to NH29 and NH17. *A*) Normalized *I–V* relations of WT rTRPV1 evoked at pH 6 in the absence (squares) and presence of 50 μM NH29 (circles). Currents were normalized to those obtained in pH 6 alone at +80 mV. (n=5). *$P < 0.05$ *vs.* pH 6 alone. *B*) Normalized *I–V* relations of WT cTRPV1 evoked at pH 6 in the absence (squares) and presence of 50 μM NH29 (circles). Currents were normalized to those obtained in pH 6 alone at +100 mV (n=5) *$P < 0.05$ *vs.* pH 6 alone. *C*) Normalized *I–V* relations of rTRPV1 in the absence (control, squares) and presence of 50 μM NH17 (circles). Currents were normalized to those obtained in control at +100 mV. (n=16). *$P < 0.01$ *vs.* control. *D*) Normalized *I–V* relations of cTRPV1 in the absence (control, squares) and presence of 50 μM NH17 (circles). Currents were normalized to those obtained in control at +100 mV (n=5). *$P < 0.05$ *vs.* control. *E*) Representative (out of 5) current trace of rTRPV1 activated by pH 6 and subsequently activated by 50 μM NH17. Cell was held at −60 mV. *F*) Representative (out of 7) current trace of cTRPV1 activated by pH 6 and subsequently exposed to 50 μM NH17. Cell was held at −60 mV. *G*) Normalized *I–V* relations of cTRPV1 evoked at pH 6 in the absence (squares) and presence of 50 μM NH17 (circles; n=7).

toxins can interact with the VSD of the same VGCC. For example, α scorpion toxins, sea anemone toxins, and some spider toxins bind to the extracellular linker S3−S4 in domain IV (receptor site 3) of voltage-gated Na^+ channels to trap the VSD in its inward position, thereby slowing the fast inactivation process (18). On the other hand, the same gating modifier toxin can promiscuously interact with different VGCCs. Thus, the spider toxin hanatoxin inhibits $K_v2.1$, $K_v4.2$ K^+ channels, or Cav2.1 Ca^{2+} channels, and more recently it was found to activate *Shaker* K_v channels (19, 33).

In this study, we showed that the diphenylamine carboxylate derivatives NH17 and NH29 exhibit target promiscuity and contrasting gating modifier properties on TRPV1 and $K_v7.2$ channels. Although NH29 acts as a $K_v7.2$ channel opener by producing a left shift of the conductance-voltage relation, it inhibits capsaicin-induced TRPV1 currents by producing a powerful right shift (+172 mV) of the channel activation curve. Whereas NH17 blocks $K_v7.2$ channels, it evokes TRPV1 currents by itself and induces a marked left shift of the conductance-voltage relation at membrane potentials negative to −40 mV. Intriguingly, NH17 has opposing actions on TRPV1 channels, exhibiting a doubly rectifying *I–V* curve. The activating effect of NH17 is sharply voltage dependent, because at potentials positive to +40 mV, NH17 inhibits TRPV1 currents. The mechanisms underlying the dual effect of NH17 are not clear. The branched tail $NH3^+$ group confers one net positive charge to NH17. An open-channel block is unlikely, as we would expect an opposite effect, with a weaker block at more depolarized potentials. It is possible that the net positive charge of NH17 locally affects the electric field, which favors the closed-channel conformation. The dramatic shifts of the TRPV1 conductance-voltage relation induced by NH29 and NH17 in opposite

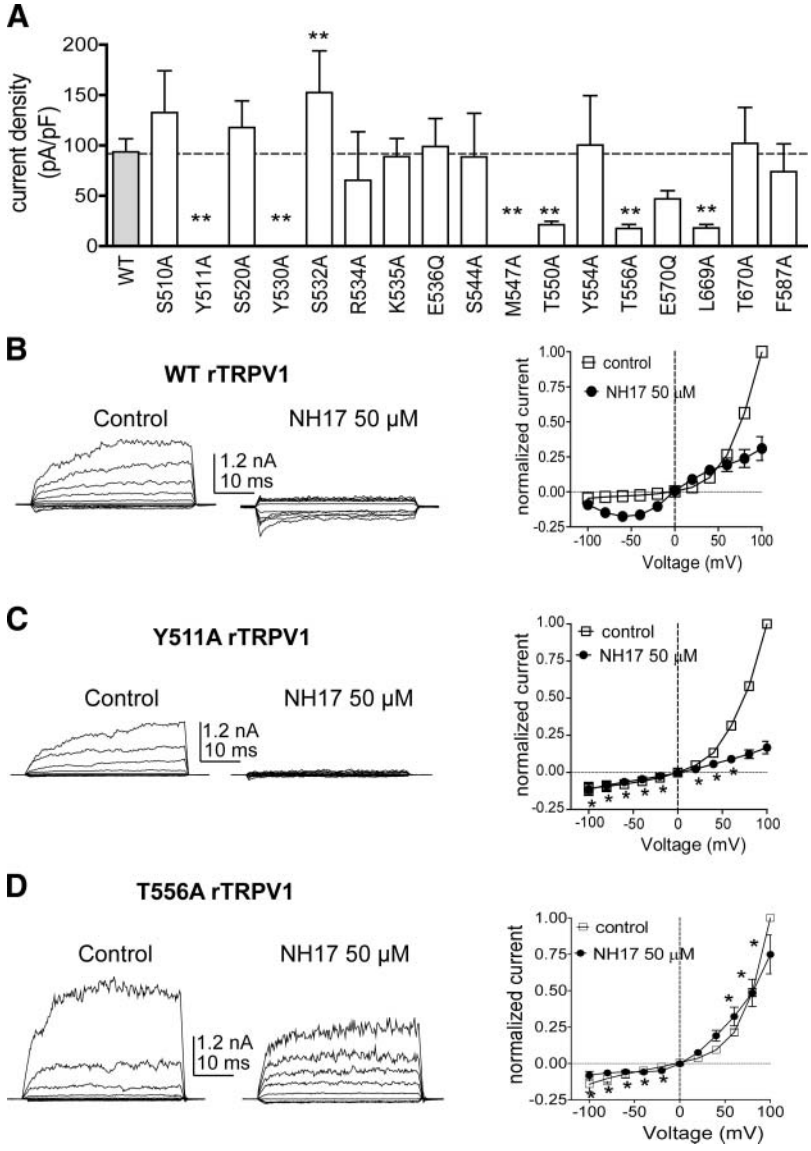

Figure 7. TRPV1 residues involved in NH17-mediated activation. *A*) Activating effect of 50 μM NH17 on WT rTRPV1 and different S3−S4 and pore mutants expressed in transfected CHO cells and measured at −60 mV (n=7–44). $^{**}P < 0.01$ *vs.* WT. *B*−*D*) Left panels: representative whole-cell currents of WT (*B*), Y511A (*C*), and T556A (*D*) rTRPV1 mutants, in the absence (control) and presence of 50 μM NH17. Cells were held at −60 mV and stepped for 40 ms from −100 mV to 100 mV in 20-mV increments. Right panels: normalized *I*–*V* relations of WT (n=16; *B*), Y511A (n=3; *C*), and T556A (n=9; *D*) rTRPV1 mutants, in the absence (open squares) and in the presence of 50 μM NH17 (solid squares). $^{*}P < 0.01$ *vs.* control.

directions, suggests that the VSDs of TRPV1 channels achieve important functions like their counterpart in classic VGCCs.

NH29 and NH17 have closely related structures, sharing the diphenylamine moiety but exhibiting different phenyl ring substituents and dissimilar branched tail groups. Our previous work suggested that in K_v7.2 channels, NH29 docks to the external groove of the VSD in a way that stabilizes the interaction between 2 conserved charged residues in S2 and S4, known to interact electrostatically, in the open state of K_v channels (21). Our present results suggest that both compounds target the VSDs of TRPV1 channels and share some of the features of the vanilloids, capsaicin and RTX. This is reflected by the loss of potency of NH29 and NH17 toward the vanilloid-insensitive cTRPV1. The important residues for ligand binding as identified by mutagenesis experiments were mapped onto the rTRPV1 structure (Fig. 8*C*). The docking data indicate that the dichloroaniline ring of NH17 and the dichloronitrophenyl ring of NH29 form a π-π stacking interaction with Tyr511, like the vanillyl moiety of capsaicin or RTX (30). When Tyr511 is mutated to alanine, it causes the loss of the π-π stacking interaction and H-bonding capabilities, leading to complete insensitivity of TRPV1 to modulation by NH17 or NH29 as well as to a significant decline in capsaicin or RTX actions (30). Glu570 and Lys571 make a hydrogen bond with NH17 and NH29, respectively. The mutation T550A may disrupt the H-bonding network, thereby leading to significant reductions in NH17 and NH29 effects. The dramatic loss of NH17-induced TRPV1 activation in mutant M547A suggests that the size or/and shape of the upper hydrophobic region of the vanilloid pocket is crucial for NH17 modulation. In addition, mutant T556A indicates that disruption of the H-bonding interaction at this position is essential for TRPV1 gating modulation by NH17. Notably, mutant L669A provides a retrospective validation for the docking model of NH17, suggesting that its branched tail $NH3^+$ group forms H-bonding interactions with the pore residue L669 in the adjacent subunit. Similarly, mutant K571A

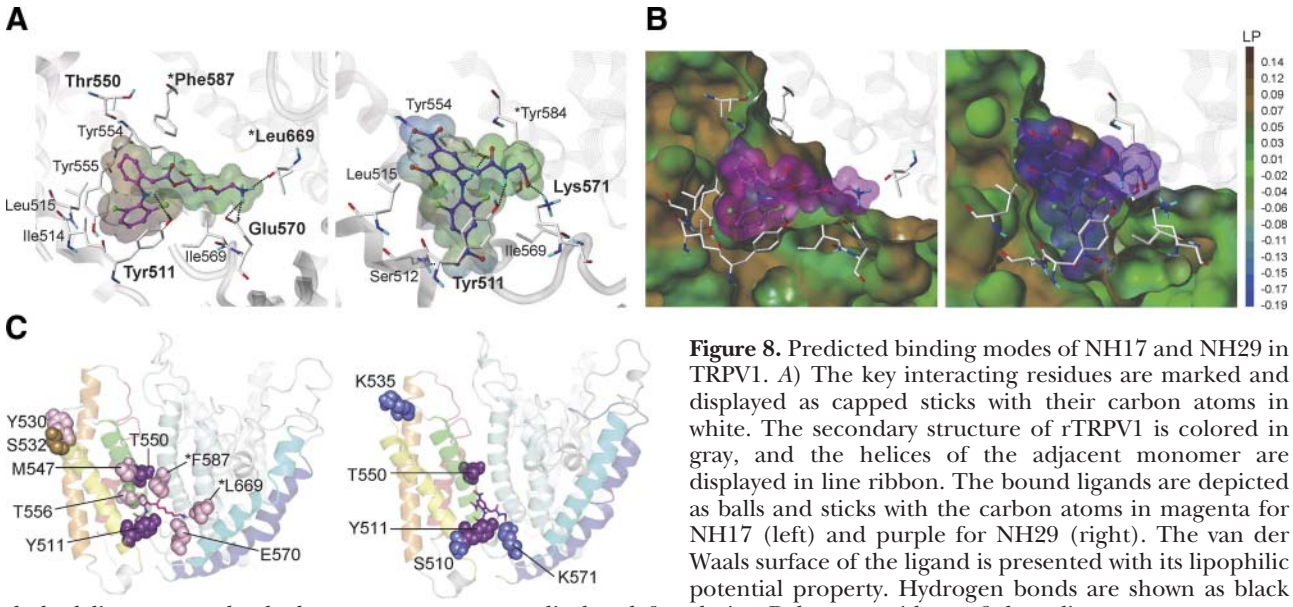

Figure 8. Predicted binding modes of NH17 and NH29 in TRPV1. *A*) The key interacting residues are marked and displayed as capped sticks with their carbon atoms in white. The secondary structure of rTRPV1 is colored in gray, and the helices of the adjacent monomer are displayed in line ribbon. The bound ligands are depicted as balls and sticks with the carbon atoms in magenta for NH17 (left) and purple for NH29 (right). The van der Waals surface of the ligand is presented with its lipophilic potential property. Hydrogen bonds are shown as black dashed lines; nonpolar hydrogen atoms are not displayed for clarity. Relevant residues of the adjacent monomer are depicted with a black asterisk *B*) Molecular surface of rTRPV1 and the bound ligands. The fast Connolly surface of rTRPV1 was generated by Molcad and colored by the lipophilic potential. The surface of rTRPV1 is *Z* clipped, and that of the ligand is in its carbon color for clarity. *C*) Structural mapping of residues that are important for ligand binding, as confirmed by mutation studies. Residues whose mutants affect the activities of NH17 (left) and NH29 (right) on rTRPV1 were displayed with spheres in purple for mutants decreasing the activities of both NH17 and NH29, in pink for mutants decreasing the activity of NH17 only, in sky blue for mutants reducing the activity of NH29 only, and in light brown for mutants increasing the activity of NH17.

retrospectively validates the binding model of NH29, suggesting that its branched tail OH group is engaged in H bonding with residue K571 in the S4−S5 linker. Tyr530, Ser532, and Lys535 appear to have long-range interactions with the capsaicin-binding site. For both compounds, we cannot exclude the possibility that additional minor binding modes could exist, notably in the upper external region of segments S3 and S4 as reflected by the different sensitivity of mutants Y530A and S532A to NH17 and mutant K535A to NH29.

Our data indicate that the same gating-modifier molecule can exert opposite effects on different VGCCs, thereby stabilizing the closed- or open-channel states. The drug promiscuity is further illustrated by the actions of NH17 and NH29 on the lone VSD proton channel mVSOP (Supplemental Fig. S2). Expression of mVSOP channels in CHO cells yielded slowly activating noninactivating proton currents (12). External exposure to NH17 (50 μM) significantly inhibited mVSOP currents by ~34%, with a significant right shift of the voltage dependence of +5.1 mV, from V_{50} = 58.9 ± 0.7 mV to V_{50} = 64.0 ± 0.8 mV (n=8, P<0.001; Supplemental Fig. S2*A*−*C*). External application of NH29 (50 μM) increased mVSOP proton currents at all potentials. The increase in mVSOP current amplitude mainly arose from a significant hyperpolarizing shift of the conductance-voltage relation (ΔV_{50}=−30.8 mV) from V_{50} = 68.5 ± 9.0 mV to V_{50} = 37.7 ± 1.4 mV (n=10, P<0.01; Supplemental Fig. S2*D*−*F*). The effects of NH29 and NH17 on mVSOP proton channels are similar to those exerted on K_v7.2 and opposite to those observed with TRPV1. Thus, structurally related yet different molecules can interact with the VSD of the same VGCC. Conversely, the same gating modifier can promiscuously interact with different VGCCs. Notably, a gating-modifier spider toxin, hanatoxin, was recently shown to exert such a dual behavior (33). In contrast to its inhibitory action on K_v2.1 channels, hanatoxin facilitates opening of the *Shaker* channel by interacting with its paddle motif (33). Hence, minute differences at the VSD-ligand interface will tune channel stabilization by the gating modifier in either the closed or the open state. In addition, lipids that were shown to bind to VSDs (15, 32) may further modulate the affect of the ligands to the channel state.

The promiscuous action of nontoxin gating-modifier molecules may in some cases be very advantageous. K_v7.2/3 and TRPV1 channels have been demonstrated to be key elements of the nociceptive pathways, displaying antagonistic activities, with TPRV1 being a strong trigger of painful stimuli that are dampened by K_v7.2/3 (34–36). Furthermore, a recent study showed that both channels physically and functionally interact *via* a macromolecular complex in which TRPV1 can suppress the activity of K_v7.2/3 (37). Molecules such as NH29 are ideally suited for dual-channel targeting, activating K_v7.2 and inhibiting TRPV1. Hence, a one-two punch strategy that targets both K_v7.2 and TRPV1 channels with the same gating modifier molecule may be of great therapeutic benefit. FJ

The authors thank Dr. David Julius (University of California–San Francisco, San Francisco, CA, USA) for rTRPV1 and cTRPV1 cDNA clones, Dr. Yasushi Okamura (Osaka Univer-

sity, Osaka, Japan) for the mVSOP clone, and the Korea Institute of Science and Technology Information (KISTI) Supercomputing Center (Yusong, Korea) for providing computing resources. This work was supported by the Deutsch-Israelische Projektkooperation (DIP) fund (Deutsche Forschungsgemeinschaft, AT 119/1-1) and the Israel Science Foundation (ISF; 488/09 to B.A.) and the National Leading Research Laboratory (NLRL) program (2011-0028885 to S.C.) funded by the Ministry of Education, Science, and Technology (MEST) and the National Research Foundation (NRF) of Korea. The authors declare no conflicts of interest.

REFERENCES

1. Ashcroft, F. M. (2000) *Ion channels and diseases*, Academic Press, San Diego, CA, USA
2. Lehmann-Horn, F., and Jurkat-Rott, K. (1999) Voltage-gated ion channels and hereditary disease. *Physiol. Rev.* **79,** 1317–1372
3. Nau, C. (2008) Voltage-gated ion channels. *Handb. Exp. Pharmacol.* **182,** 85–92
4. Yu, F. H., and Catterall, W. A. (2004) The VGL-chanome: a protein superfamily specialized for electrical signaling and ionic homeostasis. *Sci. STKE* **2004,** re15
5. Gouaux, E., and Mackinnon, R. (2005) Principles of selective ion transport in channels and pumps. *Science* **310,** 1461–1465
6. Swartz, K. J. (2004) Towards a structural view of gating in potassium channels. *Nat. Rev. Neurosci.* **5,** 905–916
7. Yellen, G. (2002) The voltage-gated potassium channels and their relatives. *Nature* **419,** 35–42
8. Yellen, G. (1998) The moving parts of voltage-gated ion channels. *Q. Rev. Biophys.* **31,** 239–295
9. Armstrong, C. M., and Bezanilla, F. (1974) Charge movement associated with the opening and closing of the activation gates of the Na channels. *J. Gen. Physiol.* **63,** 533–552
10. Murata, Y., Iwasaki, H., Sasaki, M., Inaba, K., and Okamura, Y. (2005) Phosphoinositide phosphatase activity coupled to an intrinsic voltage sensor. *Nature* **435,** 1239–1243
11. Ramsey, I. S., Moran, M. M., Chong, J. A., and Clapham, D. E. (2006) A voltage-gated proton-selective channel lacking the pore domain. *Nature* **440,** 1213–1216
12. Sasaki, M., Takagi, M., and Okamura, Y. (2006) A voltage sensor-domain protein is a voltage-gated proton channel. *Science* **312,** 589–592
13. Jiang, Y., Lee, A., Chen, J., Ruta, V., Cadene, M., Chait, B. T., and MacKinnon, R. (2003) X-ray structure of a voltage-dependent K^+ channel. *Nature* **423,** 33–41
14. Long, S. B., Campbell, E. B., and Mackinnon, R. (2005) Crystal structure of a mammalian voltage-dependent Shaker family K^+ channel. *Science* **309,** 897–903
15. Long, S. B., Tao, X., Campbell, E. B., and MacKinnon, R. (2007) Atomic structure of a voltage-dependent K^+ channel in a lipid membrane-like environment. *Nature* **450,** 376–382
16. Swartz, K. J. (2008) Sensing voltage across lipid membranes. *Nature* **456,** 891–897
17. Alabi, A. A., Bahamonde, M. I., Jung, H. J., Kim, J. I., and Swartz, K. J. (2007) Portability of paddle motif function and pharmacology in voltage sensors. *Nature* **450,** 370–375
18. Catterall, W. A., Cestele, S., Yarov-Yarovoy, V., Yu, F. H., Konoki, K., and Scheuer, T. (2007) Voltage-gated ion channels and gating modifier toxins. *Toxicon* **49,** 124–141
19. Swartz, K. J. (2007) Tarantula toxins interacting with voltage sensors in potassium channels. *Toxicon* **49,** 213–230
20. Peretz, A., Degani-Katzav, N., Talmon, M., Danieli, E., Gopin, A., Malka, E., Nachman, R., Raz, A., Shabat, D., and Attali, B. (2007) A tale of switched functions: from cyclooxygenase inhibition to m-channel modulation in new diphenylamine derivatives. *PLoS One* **2,** e1332
21. Peretz, A., Pell, L., Gofman, Y., Haitin, Y., Shamgar, L., Patrich, E., Kornilov, P., Gourgy-Hacohen, O., Ben-Tal, N., and Attali, B. (2010) Targeting the voltage sensor of Kv7.2 voltage-gated K^+ channels with a new gating-modifier. *Proc. Natl. Acad. Sci. U.S.A.* **107,** 15637–15642
22. Matta, J. A., and Ahern, G. P. (2007) Voltage is a partial activator of rat thermosensitive TRP channels. *J. Physiol.* **585,** 469–482
23. Nilius, B., Talavera, K., Owsianik, G., Prenen, J., Droogmans, G., and Voets, T. (2005) Gating of TRP channels: a voltage connection? *J. Physiol.* **567,** 35–44
24. Voets, T., Droogmans, G., Wissenbach, U., Janssens, A., Flockerzi, V., and Nilius, B. (2004) The principle of temperature-dependent gating in cold- and heat-sensitive TRP channels. *Nature* **430,** 748–754
25. Chou, M. Z., Mtui, T., Gao, Y. D., Kohler, M., and Middleton, R. E. (2004) Resiniferatoxin binds to the capsaicin receptor (TRPV1) near the extracellular side of the S4 transmembrane domain. *Biochemistry* **43,** 2501–2511
26. Gavva, N. R., Klionsky, L., Qu, Y., Shi, L., Tamir, R., Edenson, S., Zhang, T. J., Viswanadhan, V. N., Toth, A., Pearce, L. V., Vanderah, T. W., Porreca, F., Blumberg, P. M., Lile, J., Sun, Y., Wild, K., Louis, J. C., and Treanor, J. J. (2004) Molecular determinants of vanilloid sensitivity in TRPV1. *J. Biol. Chem.* **279,** 20283–20295
27. Jordt, S. E., and Julius, D. (2002) Molecular basis for species-specific sensitivity to "hot" chili peppers. *Cell* **108,** 421–430
28. Phillips, E., Reeve, A., Bevan, S., and McIntyre, P. (2004) Identification of species-specific determinants of the action of the antagonist capsazepine and the agonist PPAHV on TRPV1. *J. Biol. Chem.* **279,** 17165–17172
29. Jordt, S. E., Tominaga, M., and Julius, D. (2000) Acid potentiation of the capsaicin receptor determined by a key extracellular site. *Proc. Natl. Acad. Sci. U.S.A.* **97,** 8134–8139
30. Lee, J. H., Lee, Y., Ryu, H., Kang, D. W., Lee, J., Lazar, J., Pearce, L. V., Pavlyukovets, V. A., Blumberg, P. M., and Choi, S. (2011) Structural insights into transient receptor potential vanilloid type 1 (TRPV1) from homology modeling, flexible docking, and mutational studies. *J. Comput. Aided Mol. Des.* **25,** 317–327
31. Krepkiy, D., Gawrisch, K., and Swartz, K. J. (2012) Structural interactions between lipids, water and S1−S4 voltage-sensing domains. *J. Mol. Biol.* **423,** 632–647
32. Milescu, M., Bosmans, F., Lee, S., Alabi, A. A., Kim, J. I., and Swartz, K. J. (2009) Interactions between lipids and voltage sensor paddles detected with tarantula toxins. *Nat. Struct. Mol. Biol.* **16,** 1080–1085
33. Milescu, M., Lee, H. C., Bae, C. H., Kim, J. I., and Swartz, K. J. (2013) Opening the Shaker K^+ channel with hanatoxin. *J. Gen. Physiol.* **141,** 203–216
34. Basbaum, A. I., Bautista, D. M., Scherrer, G., and Julius, D. (2009) Cellular and molecular mechanisms of pain. *Cell* **139,** 267–284
35. Delmas, P., and Brown, D. A. (2005) Pathways modulating neural KCNQ/M (Kv7) potassium channels. *Nat. Rev. Neurosci.* **6,** 850–862
36. Jentsch, T. J. (2000) Neuronal KCNQ potassium channels: physiology and role in diseases. *Nat. Rev. Neurosci.* **1,** 21–30
37. Zhang, X. F., Han, P., Neelands, T. R., McGaraughty, S., Honore, P., Surowy, C. S., and Zhang, D. (2011) Coexpression and activation of TRPV1 suppress the activity of the KCNQ2/3 channel. *J. Gen. Physiol.* **138,** 341–352

Received for publication January 29, 2014.
Accepted for publication February 18, 2014.